HHS Public Access

Author manuscript

ACS Chem Neurosci. Author manuscript; available in PMC 2020 December 04.

Published in final edited form as:

ACS Chem Neurosci. 2020 September 02; 11(17): 2741–2752. doi:10.1021/acschemneuro.0c00376.

Amentoflavone: A Bifunctional Metal Chelator that Controls the Formation of Neurotoxic Soluble Aβ_{42} Oligomers

Liang Sun,
Department of Chemistry, University of Illinois at Urbana-Champaign, Urbana, Illinois 61801, United States

Anuj K. Sharma,
Department of Chemistry, Central University of Rajasthan, Ajmer 305801, Rajasthan, India

Byung-Hee Han,
Department of Pharmacology, A.T. Still University of Health Sciences, Kirksville, Missouri 63501, United States

Liviu M. Mirica
Department of Chemistry, University of Illinois at Urbana-Champaign, Urbana, Illinois 61801, United States; Hope Center for Neurological Disorders, Washington University School of Medicine, St. Louis, Missouri 63110, United States

Abstract

Alzheimer's disease (AD) is the most common neurodegenerative disorder, yet the cause and progression of this disorder are not completely understood. While the main hallmark of AD is the deposition of amyloid plaques consisting of the β-amyloid (Aβ) peptide, transition metal ions are also known to play a significant role in disease pathology by expediting the formation of neurotoxic soluble β-amyloid (Aβ) oligomers, reactive oxygen species (ROS), and oxidative stress. Thus, bifunctional metal chelators that can control these deleterious properties are highly desirable. Herein, we show that amentoflavone (AMF), a natural biflavonoid compound, exhibits good metal-chelating properties, especially for chelating Cu^{2+} with very high affinity ($pCu_{7.4}$ = 10.44). In addition, AMF binds to Aβ fibrils with a high affinity (K_i = 287 ± 20 nM), as revealed by a competition thioflavin T (ThT) assay, and specifically labels the amyloid plaques *ex vivo* in the brain sections of transgenic AD mice, as confirmed via immunostaining with an Aβ antibody. The effect of AMF on Aβ_{42} aggregation and disaggregation of Aβ_{42} fibrils was also investigated and revealed that AMF can control the formation of neurotoxic soluble Aβ_{42} oligomers, both in

Corresponding Author: Liviu M. Mirica - *Department of Chemistry, University of Illinois at Urbana-Champaign, Urbana, Illinois 61801, United States; Hope Center for Neurological Disorders, Washington University School of Medicine, St. Louis, Missouri 63110, United States*; mirica@illinois.edu.

Author Contributions

L.M.M. conceived the initial idea and supervised the study and the overall manuscript preparation. L.M.M., B.-H.H., and L.S. designed the *in vitro* and *in vivo* studies. L.S. and A.K.S. carried out most of the experiments and analyzed the data. L.M.M., L.S., and A.K.S. wrote the manuscript and Supporting Information, and all authors approved the final version of the manuscript for submission.

Complete contact information is available at: https://pubs.acs.org/10.1021/acschemneuro.0c00376

Supporting Information

The Supporting Information is available free of charge at https://pubs.acs.org/doi/10.1021/acschemneuro.0c00376.

Absorption and fluorescence spectra of AMF, additional brain section fluorescence images, and additional docking studies data (PDF)

The authors declare no competing financial interest.

the absence and presence of metal ions, as confirmed via cell toxicity studies. Furthermore, an ascorbate consumption assay shows that AMF exhibits potent antioxidant properties and can chelate Cu^{2+} and significantly diminish the Cu^{2+}-ascorbate redox cycling and reactive oxygen species (ROS) formation. Overall, these studies strongly suggest that AMF acts as a bifunctional chelator that can interact with various Aβ aggregates and reduce their neurotoxicity and can also bind Cu^{2+} and mediate its deleterious redox properties. Thus AMF has the potential to be a lead compound for further therapeutic agent development for AD.

Graphical Abstract

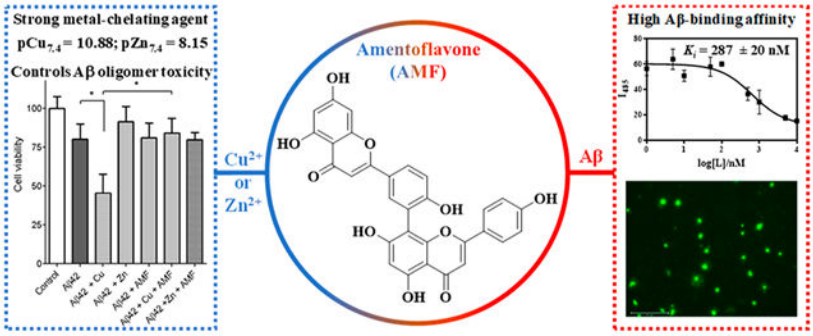

Keywords

Alzheimer’s disease; amyloid plaques; biflavonoids; metal-Aβ adducts; Aβ oligomers; oxidative stress

INTRODUCTION

Alzheimer’s disease (AD) is affecting a large fraction of the senior population all over the world, and more than five million people are affected alone in the United States.[1] Currently, there is no treatment for AD, and the unambiguous diagnosis of the disease is done by postmortem analysis of the brain. The brains of AD patients are characterized by the deposition of amyloid plaques and formation of soluble oligomers of the beta-amyloid (Aβ) peptide.[2–5] One widely employed therapeutic target has been the effective clearance of the amyloid plaques and soluble Aβ oligomers from the brain as a potential solution for AD treatment.

In addition, both *in vitro* and *in vivo* studies have shown evidence for the interaction of metal ions with Aβ aggregates, and postmortem examination of AD brains showed that copper, zinc, and iron are found in high concentrations in the amyloid plaques.[6,7] These metal ions are believed to play a key role in the amyloid aggregation process[8–16] as well as in the formation of reactive oxygen species (ROS) leading to oxidative stress.[17–22] Our studies have also recently suggested that while Cu can stabilize neurotoxic soluble Aβ oligomers,[23] Zn promotes the formation of amorphous and nontoxic Aβ aggregates.[24]

Given the mounting evidence supporting the role of transition metal ions in the pathophysiology of AD, use of metal-chelating chemical agents is emerging as a promising

treatment strategy.[3,4,25–28] Bifunctional metal chelators can interact with the Aβ species, and the metal ions are proposed to potentially be more effective therapeutics for AD.[29–36] These chelators should be able to cross the blood-brain barrier (BBB) and have to be minimally neurotoxic to be a valid method to control the onset of AD.[30] However, we have previously shown that, for the Aβ_{42} peptide, in contrast to the Aβ_{40} peptide, the previously employed strategy of inhibiting Aβ aggregation and promoting amyloid fibril disaggregation may not be optimal for the development of potential AD therapeutics, due to formation of neurotoxic soluble Aβ_{42} oligomers.[37] Thus, the development of metal chelating compounds that do not lead to formation of toxic Aβ_{42} oligomers should be promoted.[33,38] A strategy has been the search for such bifunctional chelators among naturally occurring compounds, and flavonoid compounds have been shown to interact with amyloidogenic peptides and arrest or redirect aggregation pathways.[39–46] For example, the green tea extracts (−)-epigallocatechin-3-gallate (EGCG) and myricetin inhibit metal-induced Aβ_{40} aggregation by forming EGCG-metal-Aβ_{40} complexes (Scheme 1).[39,47] We and others have previously found that the naturally occurring biflavonoids including amentoflavone (AMF) potently attenuate Aβ aggregation and cytotoxicity;[48–50] however, the metal-chelating ability of AMF and its effect on Aβ aggregation in the presence of metal ions has not been investigated to date. Herein we report a detailed investigation of metal-binding ability of AMF via spectroscopic methods and determine its metal complex stability constants, which suggest that AMF exhibits high binding affinity for Cu^{2+} versus a moderate binding affinity for Zn^{2+}. Furthermore, a Cu^{2+}-induced ascorbate consumption assay shows that AMF can significantly diminish the Cu-mediated formation of hydroxyl radicals. The effect of AMF on Aβ aggregation in the absence and presence of metal ions was also studied, to reveal that AMF reduced the formation of Cu-stabilized neurotoxic soluble Aβ_{42} oligomers. Overall, these studies strongly suggest that AMF acts as a bifunctional chelator that can interact with various Aβ aggregates and reduce their neurotoxicity, and can also bind Cu^{2+} and mediate its deleterious redox properties. Thus, AMF has the potential to be a lead compound for further therapeutic agent development for AD.

RESULTS AND DISCUSSION

Metal-Chelating Properties of AMF.

The UV-vis spectra of AMF reveal absorption bands at 275 and 360 nm (Figure S1).[51] In order to determine if AMF can interact with Cu^{2+}, various stoichiometric ratios of Cu^{2+} were added to the AMF solution. The spectral changes suggest that AMF can bind to more than one equivalent of Cu^{2+} (Figure 1). Job's plot analysis was performed to determine the AMF:Cu^{2+} stoichiometry in solution. The break in Job's plot at 0.7 mole fraction of Cu suggests that AMF can bind at least 2 equiv of Cu (Figure 1), which is in line with the proposed multiple metal ion binding sites consisting of the several ketone and phenolate groups on the adjacent rings of AMF (Figure S3).[51]

Since AMF contains phenol and ketone groups that can undergo protonation and deprotonation, the acidity constants (pK_a) of AMF were determined using UV-vis spectrophotometric titrations. The UV-vis titrations from pH 3.0 to 11.0 reveal several changes in the spectra (Figure 2), and the best fit to the data was obtained with five pK_a

values: 1.42, 4.57, 7.61, 8.71, and 10.96. Based on previously reported acidity constants for various phenols, we assigned the lowest pK_a value to the protonation of one keto group, the next two pK_a values to the deprotonation of the *o*-carbonyl-phenol groups, for which the corresponding conjugate base is stabilized by conjugation similar to acetylacetone (Hacac),[52] and the highest two pK_a values are likely due to deprotonation of phenol groups in AMF.

Metal Complex Stability Constants Determination.

We then performed spectropotentiometric titrations of AMF in the presence of Cu^{2+} and Zn^{2+} ions to determine the corresponding metal complex stability constants. In the presence of Cu^{2+}, the absorption band at 350 nm decreases regularly in the pH 3–8 range (Figure 3). At higher pH values (pH 8–12), a species with a broad absorption band at 400 nm slowly increases. The data was fitted with the HYPSPEC program using a 2:1 Cu:AMF stoichiometry and the presence of only two species was observed: Cu_2LH and Cu_2L, which matches the stoichiometry suggested by the Job's plot analysis. The obtained stability constant of 32.53 for the Cu_2(AMF) complex formation suggests that AMF has a very strong affinity for Cu (Table 1). In the presence of Zn^{2+}, the complex formation was observed from pH 3 to 9, but at higher pH some free ligand was observed based on spectral similarity (Figure 4). The data fitting and stability constants value of 24.96 of Zn_2(AMF) formation (Table 1) suggest a reasonable strong affinity for Zn albeit much lower than that for Cu. Since the stability constants are a measure of the overall stability of a metal-ligand complex and do not reflect the metal-binding affinity of ligands at a specific pH value,[37,53] a better comparison between different metal complexes can be obtained by comparing the concentration of unchelated metal ions pM, where pM = $-\log[M_{unchelated}]$. Using the acidity and stability constants obtained from the data fits, pM values were obtained for the AMF: Zn system at pH 7.4 and for the AMF:Cu system at pH 6.6 and 7.4 (Table 2).[53] The higher pM values obtained for the AMF:Cu system (10.44 at pH 7.4 and 9.62 at pH 6.6) suggests that AMF is a surprisingly strong chelator for Cu^{2+}, similarly to commonly used Cu chelators such as DTPA.[54]

Binding Affinity of AMF for Aβ Fibrils.

Naturally occurring flavonoids have previously been shown to interact with amyloidogenic peptides and control the aggregation process.[39,55,56] However, the direct determination of the binding affinities toward Aβ fibrils using fluorescence assays has not been employed for such natural products. Therefore, we have performed Thioflavin T (ThT) competition assays using Aβ fibrils, and AMF (0–10 μM) was added to solutions containing Aβ fibrils and ThT and a decrease in the ThT fluorescence intensity was recorded within a few minutes. We consider that AMF should not affect nature of the Aβ fibrils in such a short period of time (see below), and thus, the main reason for the reduction in fluorescence intensity is that AMF replaces the ThT molecules that bind to the amyloid fibrils. Fitting of the data using a one-site competitive binding model suggests a K_i = 287 ± 20 nM affinity of AMF toward Aβ fibrils (Figure 5), a value that is very similar to the IC_{50} value reported recently for the inhibition of Aβ_{42} fibrillization.[50]

Molecular Docking Studies.

In order to better understand the interaction of AMF with the Aβ aggregates, we performed a series of docking studies using the Schrödinger program Glide[57] and different Aβ aggregate structures from the RCSB database: the Aβ_{42} tetramers (PDB ID: 6RHY) were used as a working model for the toxic Aβ oligomers associated with cell membrane disruption in AD[58] as well as the Aβ_{40} fibrils (PDB ID: 2M4J) and the Aβ_{42} fibrils (PDB ID: 5OQV) structures. In order to select the best poses for each aggregate structures, the conformations of the AMF-Aβ species adducts were ranked by the docking score and the Glide e-model energy. For the AMF-Aβ_{42} tetramer adducts, the structures that have the best docking scores show that AMF mainly interacts through hydrogen bonds with the phenol groups with the hydrophilic amino acid residues such as Asp-1, His-6, and Asp-7 located at the N-terminus and outside of the hydrophobic core (Figure 6a). Importantly, several reports have shown that when Cu^{2+} ions bind to the Aβ peptides, the N-terminus amino acids such as Asp-1, His-6, His-13, or His-14 can strongly chelate the Cu^{2+} ions to form Cu^{2+}-Aβ species,[59] suggesting that AMF may have the ability to modulate the Cu^{2+}-mediated stabilization of soluble Aβ oligomers (*vide infra*). While the other evaluated poses show interactions of AMF with other residues of the such as Glu-3, Asp-7, Tyr-10, Gln-15, and Glu-22 (Figures 6a and S6), all these residues are hydrophilic and could interact with metal ions such as Cu^{2+}, and therefore, AMF could modulate the Cu^{2+}-Aβ oligomers interactions.[51] When docked onto the Aβ_{40} fibril structure, AMF is positioned near the KLVFF hydrophobic core and interacts via $\pi-\pi$ interactions with the Phe-19 and Phe-20 residues and via hydrogen bonds with Gln-15, Leu-17, and Lys-28. Interestingly, the KLVFF core is also proposed to be the binding site for Thioflavin T,[60] thus suggesting AMF can replace ThT efficiently and in line with the results obtained from the ThT fluorescence competition assays (Figures 6b and S5b).[51] When docked onto the Aβ_{42} fibril structure, AMF interacts with the Cu-binding amino acid residues such as Glu-3 and His-6 (Figure 6c), further indicating that AMF may have the capability to modulate the interaction between Cu^{2+} and the Aβ_{42} fibrils (*vide infra*). Although the binding sites for AMF are slightly different for the Aβ_{40} vs the Aβ_{42} fibrils, in both cases the AMF selectively binds to the groove located on the terminus of the axis of fibril growth, which may explain why AMF can mitigate the growth of the Aβ fibrils. Moreover, comparing among these AMF-Aβ adducts, the best docking score and Glide e-model energy are comparable when AMF binds to the Aβ oligomers and fibrils, suggesting that AMF can interact similarly with these types of Aβ aggregates (Table S1).[51]

Fluorescence Staining of 5xFAD Mouse Brain Sections.

To further probe the ability of AMF to interact with various Aβ aggregates, we took advantage of the intrinsic fluorescence properties of AMF (Figure S2) to stain the native amyloid plaques present in the brain sections of 7 month old 5xFAD transgenic mice. These brain sections were first stained with AMF, followed by immunostaining with the HJ3.4 antibody that can bind to a wide range of Aβ species.[61] Excitingly, AMF exhibits strong fluorescent intensity on the stained 5xFAD mouse brain sections that shows good colocalization with the immunofluorescence of HJ3.4 (Pearson's correlation coefficient = 0.65, Figure 7), suggesting that AMF can bind to the amyloid plaques, especially to the dense core of the amyloid plaques when compared to the HJ3.4 antibody. Moreover, we have also stained the 5xFAD brain sections with the Cu^{2+}-AMF and Zn^{2+}-AMF complexes,

followed by immunostaining with the HJ3.4 antibody. For the Zn^{2+}-AMF adduct, a low fluorescence intensity is observed, indicating that either this complex exhibits quenched fluorescence or that it cannot specifically bind to the amyloid plaques (Figure S4).[51] However, staining of the 5xFAD brain sections with the Cu^{2+}-AMF adduct shows very good colocalization with HJ3.4 (Pearson's correlation coefficient = 0.83, Figure 7), indicating that Cu^{2+}-AMF can selectively bind to the amyloid plaques *ex vivo.* It is important to note that the absolute fluorescence intensity of the Cu^{2+}-AMF amyloid plaque staining was significantly reduced vs staining with AMF alone, likely due to the fluorescence quenching ability of the Cu^{2+} ions. Also, no appreciable autofluorescence from the amyloid plaques was observed, either in the FITC or the Texas Red channel (Figure S5).

The Effect of AMF on Aβ_{42} Aggregation.

We then investigated the effect of AMF on Aβ aggregation, both in the presence and absence of metal ions. For this purpose, we have used the Aβ_{42} peptide, which was also shown to form neurotoxic soluble Aβ oligomers.[62–66] To study the inhibitory effect of AMF on Aβ aggregation, freshly prepared monomeric Aβ_{42} solutions were treated with metal ions, AMF, or both.[37] Interestingly, the ThT fluorescence assays reveal that AMF dramatically reduced the fibrillization of Aβ_{42}, both in presence and absence of Cu^{2+} or Zn^{2+} (Figure 8).[67]

To further study the effect of AMF on Aβ_{42} aggregation, native gel electrophoresis/Western blot analysis and transmission electron microscopy (TEM) were used as these techniques provide a more in-depth analysis of the various size Aβ aggregates formed. Similar to previous reports, Aβ_{42} forms fibrils within 24 h of incubation, while the presence of Cu^{2+} generates a range of soluble Aβ_{42} oligomers, and the presence of Zn^{2+} leads to amorphous Aβ_{42} aggregates (Figures 9a–c and S7).[24,37] Interestingly, the presence of AMF arrests the Aβ_{42} aggregation process and only small amorphous aggregates were observed by TEM, both in the absence and presence of Cu^{2+} (Figure 9d and e), while in the presence of Zn^{2+} and AMF a range of amorphous and fibrillar aggregates is formed (Figure 9f). The native gel/Western blot further supports that AMF dramatically reduces the amount of large Aβ_{42} aggregates, while in the presence of Cu^{2+} the amount of soluble Aβ_{42} oligomers is also reduced, and in the presence of AMF and Zn^{2+} a wide range of various-size aggregates is formed (Figure 9).

The Effect of AMF on Disaggregation of Aβ Fibrils.

Inspired by the inhibition of Aβ_{42} aggregation results, we then investigated the ability of AMF to disaggregate the preformed Aβ_{42} fibrils, in the presence or absence of metal ions. The Aβ_{42} fibrils (prepared by incubating for 24 h at 37 °C) were incubated with AMF for an additional 24 h at 37 °C, and the extent of disaggregation in these samples was evaluated by ThT fluorescence, TEM, and native gel/Western blotting. The ThT fluorescence results were similar to those obtained in the inhibition of Aβ_{42} aggregation experiments and show that AMF is efficient at reducing the amount of Aβ_{42} fibrils, both in the absence and presence of Cu^{2+} ions (Figure 10).

The TEM and native gel/Western blot analyses also yield similar results to those obtained from the inhibition of Aβ_{42} aggregation studies. While the 48 h incubation gives mature

Aβ_{42} fibrils, the presence of Cu^{2+} stabilizes a range of soluble Aβ_{42} oligomers and the presence of Zn^{2+} leads to wide range of amorphous aggregates (Figure 11a–c). The addition of AMF disaggregates the Aβ_{42} fibrils efficiently, and only a reduced amount of amorphous smaller aggregates is observed (Figure 11d). Excitingly, the addition of AMF to the Cu^{2+}-incubated Aβ_{42} aggregates shows the reduction in the amount of both large aggregates and smaller Aβ_{42} oligomers (Figure 11e), while the amount of Zn^{2+}-incubated Aβ_{42} amorphous aggregates also decreases to some extent upon the addition of AMF (Figure 11f). Overall, both the inhibition of Aβ_{42} and disaggregation of Aβ_{42} fibrils studies strongly suggest that AMF is a good agent for inhibition of Aβ aggregation as well as for disaggregating the preformed Aβ aggregates. Moreover, in the presence of Cu^{2+} ions, the amount of soluble Aβ_{42} oligomers is also reduced by AMF, which is a desirable property targeted in the development of Aβ-binding and metal-chelating bifunctional compounds.[37]

Cu^{2+}-Induced Ascorbate Consumption Assays.

It has been shown previously that Aβ_{42} species can bind Cu^{2+} and promote its reduction to Cu^{+}, which can react with dioxygen to generate reactive oxygen species (ROS) and lead to oxidative stress *in vivo*.[68,69] Herein, we have employed an ascorbate consumption assay to evaluate the ability of AMF to suppress the Cu^{2+}-ascorbate redox cycling. In the absence of any other additives, the consumption of ascorbate in the presence of Cu^{2+} is rapid (Figure 12a, black).[51] However, if Cu^{2+} is premixed with 2 equiv of AMF, the ascorbate consumption is dramatically reduced (Figure 12a, red),[51] indicating that the AMF can bind tightly to Cu^{2+} and mitigate its reduction to Cu^{2+}, thus acting as an antioxidant and arrest the redox cycling. Furthermore, when 2 equiv AMF was added into the Cu^{2+}-ascorbate solution, the consumption of ascorbate is rapidly reduced significantly (Figure 12a, blue),[51] showing that AMF can alleviate the Cu^{2+}-ascorbate redox cycling even when it was not premixed with Cu^{2+}.

We have also investigated ascorbate consumption in the presence of monomeric Aβ_{42}, mimicking the conditions that are more relevant to AD. Compared with the Cu^{2+}-Aβ_{42} species that rapidly lead to consumption of ascorbate through redox cycling (Figure 12b, black),[51] the presence of the premixed AMF-Cu^{2+} complex leads to a significant inhibition of the ascorbate consumption (Figure 12b, red),[51] indicating that Aβ_{42} cannot outcompete AMF for binding to the Cu^{2+} ions. Moreover, when AMF added to the Cu^{2+}-Aβ_{42}-ascorbate solution, it was able efficiently reduce the consumption of ascorbate via the Cu^{2+}-ascorbate redox cycling even in the presence of Aβ_{42} species (Figure 12b, blue),[51] suggesting that AMF can outcompete Aβ_{42} for binding to the Cu^{2+} ions. Overall, these results strongly suggest that AMF has potent antioxidant properties and can efficiently chelate the Cu^{2+} ions to prevent the reduction by ascorbate, even with the presence of Aβ_{42} species, and thus inhibit the formation of ROS during the Cu^{2+}-ascorbate redox cycling.

Cell Toxicity Studies.

Since it was recently shown that the Cu^{2+} ions can promote the formation of neurotoxic soluble Aβ oligomers,[24,70] 42 we have investigated whether AMF can modulate the formation of such Cu^{2+}-stabilized soluble Aβ_{42} oligomers. First, the Neuro2A cells were treated with the Aβ_{42} fibrils that lead to some neurotoxicity (80 ± 5% cell viability)

compared with the DMSO control, while the Cu^{2+}-stabilized Aβ_{42} oligomers showed a significantly increased cytotoxicity (60 ± 2% cell viability) *vs* the Aβ_{42} fibrils (Figure 13, top).[24] The presence of Zn^{2+} did not significantly affect the Aβ_{42} cytotoxicity. Excitingly, the addition of AMF significantly attenuates the cytotoxicity of the Cu^{2+}-stabilized Aβ_{42} oligomers (85 ± 5% cell viability), further suggesting that AMF can mitigate the interaction of Cu^{2+} with the Aβ_{42} species. Next, we have examined the cytotoxicity of the preformed Aβ_{42} aggregates (Figure 13, bottom). While the Aβ_{42} aggregates formed in the presence of Cu^{2+} ions dramatically increased the cytotoxicity compared to the Aβ_{42} fibrils alone (45 ± 8% versus 79 ± 8% cell viability, respectively), the addition of AMF significantly reduced cytotoxicity of the Cu^{2+}-containing Aβ_{42} aggregates (83 ± 7% cell viability). To the best of our knowledge, these results suggest for the first time that AMF can act as a bifunctional chelator and mitigate the neurotoxicity of Cu^{2+}-Aβ_{42} species in a cellular assay.

CONCLUSIONS

In summary, herein we report that amentoflavone (AMF), a naturally occurring biflavonoid compound, exhibits good metal-chelating properties, especially for binding Cu^{2+} with a very high affinity ($pCu_{7.4}$ = 10.44), as shown via spectropotentiometric titrations. In addition, AMF binds to Aβ fibrils with a high affinity (K_i = 287 ± 20 nM), as revealed by a competition thioflavin T (ThT) assay, and specifically labels the amyloid plaques *ex vivo* in the brain sections of transgenic 5xFAD mice, as confirmed via immunostaining with an Aβ antibody. The effect of AMF on Aβ_{42} aggregation and disaggregation of Aβ_{42} fibrils was also investigated, to reveal that AMF can control the cytotoxicity of Aβ_{42} aggregates, especially the marked neurotoxicity of the Cu^{2+}-stabilized soluble Aβ_{42} oligomers. Furthermore, a Cu^{2+}-induced ascorbate consumption assay shows that AMF exhibits potent antioxidant properties and can chelate Cu^{2+} and significantly diminish its reduction and Cu^{2+}-ascorbate redox cycling and ROS formation. Overall, these studies strongly suggest that AMF acts as a bifunctional chelator that can interact with various Aβ aggregates and reduce their neurotoxicity and can also bind Cu^{2+} and mediate its deleterious redox properties. Thus, AMF has the potential to be a lead compound for further therapeutic agent development for AD.

METHODS

All reagents were purchased from commercial sources and used as received unless stated otherwise. AMF was obtained from Sigma-Aldrich. All solutions and buffers were prepared using metal-free Millipore water that was treated with Chelex overnight and filtered through a 0.22 μm nylon filter. UV-visible spectra were recorded on a Varian Cary 50 Bio spectrophotometer and are reported as λ_{max}, nm (ε, M^{-1} cm^{-1}). The monoclonal anti-Aβ antibody HJ3.4 was obtained from Prof. David Holtzman (Department of Neurology, Washington University School of Medicine). The primary antibodies were labeled with the CF594 fluorescent dye by using the Mix-n-Stain CF 594 Antibody Labeling Kit (Sigma-Aldrich), in accordance with the protocol provided by the manufacturer. All animal studies have been approved by the Washington University Animal Studies Committee, and the handling of mice was performed in accordance with institutional regulations.

Acidity and Stability Constant Determination.

UV-vis pH titrations were employed for the determination of acidity constants of AMF and its stability constants with Cu^{2+} and Zn^{2+}. For the acidity constants determinations, solutions of AMF (25 μM, 0.1 M NaCl, pH 3) were titrated with small aliquots of 0.1 M NaOH at room temperature under N_2. At least 30 UV-vis spectra were collected in the pH 3–11 range. DMSO stock solutions (5 mM) were diluted in EtOH-water mixtures in which EtOH did not exceed 10% (v:v). Similarly, the metal complex stability constants were determined by titrating solutions of AMF and $Cu(ClO_4)_2 \cdot 6H_2O$ or $Zn(ClO_4)_2 \cdot 6H_2O$ with small aliquots of 0.1 M NaOH at room temperature. At least 30 UV-vis spectra were collected in the pH 3–11 range. The acidity and stability constants were calculated using the HypSpec program (Protonic Software, UK),[71] and speciation plots of the compounds and their metal complexes were calculated using the program HySS2009 (Protonic Software, UK).[72]

Amyloid β Peptide Experiments.

Aβ monomeric films were prepared by dissolving commercial Aβ_{42} (or Aβ_{40} for Aβ fibril-binding studies) peptide (Keck Biotechnology Resource Laboratory, Yale University) in HFIP (1 mM) and incubating for 1 h at room temperature.[73] This solution was then aliquoted out and evaporated overnight. The aliquots were vacuum centrifuged, and the resulting monomeric films stored at −80 °C. Aβ fibrils were generated by dissolving monomeric Aβ films in DMSO, diluting into the appropriate buffer, and incubating for 24 h at 37 °C with continuous agitation (final DMSO concentration was <2%). For metal-containing fibrils, the corresponding metal ions were added before the initiation of the aggregation conditions. For the inhibition studies, AMF (25 μM) was added to Aβ solutions (25 μM) in the absence or presence of metal salts ($CuCl_2$ or $ZnCl_2$, 25 μM) and incubated for 24 h at 37 °C with constant agitation. For the disaggregation studies, the preformed Aβ fibrils in the absence or presence of metal ions were treated with AMF and incubated for 24 h at 37 °C with constant agitation. For the preparation of soluble Aβ_{42} oligomers a literature protocol was followed.[74,75] A monomeric film of Aβ_{42} was dissolved in anhydrous DMSO, followed by addition of DMEM-F12 media (1:1 v:v, without phenol red, Invitrogen). The solution (50–100 μM) was incubated at 4 °C for 24 h and then centrifuged at 10,000 g for 10 min. The supernatant was used as a solution of soluble Aβ_{42} oligomers.

Histological Staining of 5xFAD Mice Brain Sections.

Brain sections obtained from 7 month old transgenic 5xFAD mice were washed with PBS (3 × 5 min) and blocked with bovine serum albumin (2% BSA in PBS, pH 7.4, 10 min). Then the sections were incubated with 25 μM AMF or metal-AMF solutions and then sequentially stained with the CF594-labeled HJ3.4 antibody (1 μg/mL) for 1 h. The brain sections were treated with 2% BSA-PBS for 4 min to remove any compounds or antibodies that were nonspecifically binding to the tissue. Finally, the sections were washed with PBS (3 × 2 min) and Millipore water (2 min) and then mounted with a coverslip and Vectashield mounting medium. The stained brain sections were analyzed using an EVOS FL Auto 2 fluorescence microscope. The fluorescence images of the AMF/Cu-AMF complex staining and CF594-labeled HJ3.4 antibody immunostaining were separately imaged in the FITC and Texas Red

channels, respectively. The visualization and determination of the Pearson's correlation coefficients were performed using the imaging software Fiji (ImageJ 1.52p).

Molecular Docking.

The Schrödinger Suite was used to predict the docking posed and the binding interactions of AMF with the structure of various Aβ aggregates from the RCSB database. The Aβ aggregates used for docking are the Aβ_{42} tetramers (PDB ID: 6RHY),[58] the Aβ_{40} fibrils (PDB ID: 2M4J)[76] and the Aβ_{42} fibrils (PDB ID: 5OQV).[77] The AMF molecule was prepared for docking using Ligprep, and the pH was set as 7.0 ± 2.0 using Epik. The four different protonation states of AMF were obtained from the preparation of the ligand and used for the docking studies. The three Aβ aggregate structures were processed by minimal minimization with the OPLS3 force field using the Protein Preparation Wizard program. The grid size was set to 36 Å in each direction to include all amino acid sequences. The molecular docking was performed using Glide.[78] The four best poses obtained for each Aβ aggregate structure were ranked by both the docking score and Glide e-model energy, and the structures with the best docking scores and Glide e-model energies were rendered in PyMol.[79]

Fluorescence Measurements.

All fluorescence measurements were performed using a SpectraMax M2e plate reader (Molecular Devices). For the ThT fluorescence studies, the samples were diluted to a final concentration of 2.5 μM Aβ in PBS containing 10 μM ThT and the fluorescence measured at 485 nm (λ_{ex} = 435 nm). For the Aβ fibril binding studies in a Thioflavin T (ThT) competition assay, the Aβ (1 μM) fibril solution with ThT (2 μM) was titrated with small amounts of AMF and the decrease in ThT fluorescence was measured ($\lambda_{ex}/\lambda_{em}$ = 435/485 nm). For calculating K_i values, a K_d value of 1.17 μM was used for the binding of ThT to Aβ_{40} fibrils, as determined previously.[24,37]

Transmission Electron Microscopy (TEM).

Glow-discharged grids (Formvar/Carbon 300 mesh, Electron Microscopy Sciences) were treated with Aβ samples (25 μM, 5 μL) for 5 min at room temperature. The excess solution was removed using filter paper, and the grids were rinsed twice with H_2O (5 μL), stained with uranyl acetate (1% w/v, H_2O, 5 μL) for 1 min, blotted with filter paper, and dried for 15 min at room temperature. Images were captured using a FEI G2 Spirit Twin microscope (60–80 kV, 6500–97 000× magnification) at the Nano Research Facility (NRF) at Washington University in St. Louis, MO.

Native Gel Electrophoresis and Western Blotting.

All gels, buffers, membranes, and other reagents were purchased from Invitrogen and used as directed except where otherwise noted. Samples were separated on 10–20% gradient Tris-tricine mini gels. The gel was transferred to a nitrocellulose membrane in an ice bath and the protocol was followed as suggested except that the membrane was blocked overnight at 4 °C. After blocking, the membrane was incubated in a solution (1:2000 dilutions) of 6E10 anti-Aβ primary antibody (Covance) for 3 h. Invitrogen's Western Breeze Chem-

iluminescent kit was used to visualize the bands. An alkaline-phosphatase antimouse secondary antibody was used, and the protein bands were imaged using a FUJIFILM Luminescent Image Analyzer LAS-1000CH.

Cu^{2+}-Induced Ascorbate Consumption Assays.

A 10 mM stock solution of sodium ascorbate was prepared in 10 mM PBS buffer, and a 10 mM stock solution of $CuSO_4$ was prepared in Millipore water. A 4 mM AMF stock solution was prepared in DMSO. Monomeric Aβ_{42} was dissolved in PBS buffer to make a 100 μM stock solution. Final concentrations in the assay were as follows: 100 μM ascorbate, 10 μM $CuSO_4$, 12 μM Aβ_{42}, and 24 μM AMF. For the assays without the Aβ peptide, three different conditions were employed as follows: (1) ascorbate was first added into the PBS buffer following by the addition of $CuSO_4$ solution; (2) the AMF solution was premixed with the $CuSO_4$ solution for 30 min, and then this was added to the ascorbate solution; (3) ascorbate was first added into the PBS buffer followed by the addition of $CuSO_4$ solution, and then when the absorbance at 265 nm reached half of that at the starting point, AMF was added to the solution. The solutions were monitored at 265 nm for 40 min, and spectra were collect every 30 s. The same conditions were used for the assays in the presence of 12 μM Aβ_{42}.

Cytotoxicity Studies.

Cytotoxicity studies were performed according to our published protocol using the Alamar Blue assay.[24,37] Mouse neuroblastoma Neuro2A (N2A) cells were purchased from the American Type Culture Collection. Cells were grown in Dulbecco's modified Eagle's medium (DMEM; Gibco) supplemented with 10% fetal bovine serum and antibiotics at 37 °C in a humidified 5% CO_2 incubator. N2A cells were suspended in the medium and seeded into a 96-well plate (2.5×10^4 cells/well). At 24 h later, cells were washed with DMEM/N2 medium (Gibco) and treated with Aβ_{42} species, AMF, and metal ions in a final volume of 100 μL. After an additional incubation of 40 h, Alamar blue (Resazurin; Sigma-Aldrich) was added to each well at a final concentration of 30 μg/mL and incubated at 37 °C for 90 min, the absorbance was read at 570 nm, and the cell viability was calculated.

Supplementary Material

Refer to Web version on PubMed Central for supplementary material.

ACKNOWLEDGMENTS

This work was supported by research funding from the NIH (R01GM114588 to L.M.M.) and the Alzheimer's Association (NIRG 12-259199 to L.M.M.).

REFERENCES

(1). Alzheimer's Association (2020) Alzheimer's disease facts and figures. Alzheimer's Dementia 16, 391–460.

(2). Hardy J, and Selkoe DJ (2002) The Amyloid Hypothesis of Alzheimer's Disease: Progress and Problems on the Road to Therapeutics. Science 297 (5580), 353–356. [PubMed: 12130773]

(3). DeToma AS, Salamekh S, Ramamoorthy A, and Lim MH (2012) Misfolded proteins in Alzheimer's disease and type II diabetes. Chem. Soc. Rev 41 (2), 608–21. [PubMed: 21818468]

(4). Kepp KP (2012) Bioinorganic chemistry of Alzheimer's disease. Chem. Rev 112 (10), 5193–5239. [PubMed: 22793492]

(5). Jakob-Roetne R, and Jacobsen H (2009) Alzheimer's Disease: From Pathology to Therapeutic Approaches. Angew. Chem., Int. Ed 48 (17), 3030–3059.

(6). Bush AI, Pettingell WH, Multhaup G, Paradis MD, Vonsattel JP, Gusella JF, Beyreuther K, Masters CL, and Tanzi RE (1994) Rapid Induction of Alzheimer a-Beta Amyloid Formation by Zinc. Science 265 (5177), 1464–1467. [PubMed: 8073293]

(7). Atwood CS, Moir RD, Huang XD, Scarpa RC, Bacarra NME, Romano DM, Hartshorn MK, Tanzi RE, and Bush AI (1998) Dramatic aggregation of Alzheimer A beta by Cu(II) is induced by conditions representing physiological acidosis. J. Biol. Chem 273 (21), 12817–12826. [PubMed: 9582309]

(8). Rana M, and Sharma AK (2019) Cu and Zn interactions with Abeta peptides: consequence of coordination on aggregation and formation of neurotoxic soluble Abeta oligomers. Metallomics 11 (1), 64–84. [PubMed: 30234208]

(9). Lovell MA, Robertson JD, Teesdale WJ, Campbell JL, and Markesbery WR (1998) Copper, iron and zinc in Alzheimer's disease senile plaques. J. Neurol. Sci 158 (1), 47–52. [PubMed: 9667777]

(10). Faller P (2009) Copper and Zinc Binding to Amyloid-β: Coordination, Dynamics, Aggregation, Reactivity and Metal-Ion Transfer. ChemBioChem 10 (18), 2837–2845. [PubMed: 19877000]

(11). Zatta P, Drago D, Bolognin S, and Sensi SL (2009) Alzheimer's disease, metal ions and metal homeostatic therapy. Trends Pharmacol. Sci 30 (7), 346–355. [PubMed: 19540003]

(12). Bagheri S, Squitti R, Haertle T, Siotto M, and Saboury AA (2018) Role of Copper in the Onset of Alzheimer's Disease Compared to Other Metals. Front. Aging Neurosci 9, 446. [PubMed: 29472855]

(13). Faller P, and Hureau C (2009) Bioinorganic chemistry of copper and zinc ions coordinated to amyloid-β peptide. Dalton Trans. 38 (7), 1080–1094.

(14). Kepp KP (2017) Alzheimer's disease: How metal ions define β-amyloid function. Coord. Chem. Rev 351, 127–159.

(15). Atrian-Blasco E, Gonzalez P, Santoro A, Alies B, Faller P, and Hureau C (2018) Cu and Zn coordination to amyloid peptides: From fascinating chemistry to debated pathological relevance. Coord. Chem. Rev 371, 38–55.

(16). Abeyawardhane DL, Fernandez RD, Murgas CJ, Heitger DR, Forney AK, Crozier MK, and Lucas HR (2018) Iron Redox Chemistry Promotes Antiparallel Oligomerization of alpha-Synuclein. J. Am. Chem. Soc 140 (15), 5028–5032. [PubMed: 29608844]

(17). Zhu X, Su B, Wang X, Smith M, and Perry G (2007) Causes of oxidative stress in Alzheimer disease. Cell. Mol. Life Sci 64 (17), 2202–2210. [PubMed: 17605000]

(18). Crichton RR, Dexter DT, and Ward RJ (2008) Metal based neurodegenerative diseases—From molecular mechanisms to therapeutic strategies. Coord. Chem. Rev 252 (10–11), 1189–1199.

(19). Cheignon C, Tomas M, Bonnefont-Rousselot D, Faller P, Hureau C, and Collin F (2018) Oxidative stress and the amyloid beta peptide in Alzheimer's disease. Redox Biol. 14, 450–464. [PubMed: 29080524]

(20). Tonnies E, and Trushina E (2017) Oxidative Stress, Synaptic Dysfunction, and Alzheimer's Disease. J. Alzheimer's Dis 57 (4), 1105–1121. [PubMed: 28059794]

(21). Hureau C, and Faller P (2009) Aβ-mediated ROS production by Cu ions: structural insights, mechanisms and relevance to Alzheimer's disease. Biochimie 91 (10), 1212–1217. [PubMed: 19332103]

(22). Cheignon C, Jones M, Atrian-Blasco E, Kieffer I, Faller P, Collin F, and Hureau C (2017) Identification of key structural features of the elusive Cu-Abeta complex that generates ROS in Alzheimer's disease. Chem. Sci 8 (7), 5107–5118. [PubMed: 28970897]

(23). Zhang Y, Rempel DL, Zhang J, Sharma AK, Mirica LM, and Gross ML (2013) Pulsed hydrogen-deuterium exchange mass spectrometry probes conformational changes in amyloid beta (Aβ) peptide aggregation. Proc. Natl. Acad. Sci. U. S. A 110, 14604–14609. [PubMed: 23959898]

(24). Sharma AK, Pavlova ST, Kim J, Kim J, and Mirica LM (2013) The effect of Cu^{2+} and Zn^{2+} on the Aβ_{42} peptide aggregation and cellular toxicity. Metallomics 5 (11), 1529–1536. [PubMed: 23995980]

(25). Que EL, Domaille DW, and Chang CJ (2008) Metals in neurobiology: probing their chemistry and biology with molecular imaging. Chem. Rev 108 (5), 1517–1549. [PubMed: 18426241]

(26). Esmieu C, Guettas D, Conte-Daban A, Sabater L, Faller P, and Hureau C (2019) Copper-Targeting Approaches in Alzheimer's Disease: How To Improve the Fallouts Obtained from in Vitro Studies. Inorg. Chem 58 (20), 13509–13527. [PubMed: 31247877]

(27). Faller P, Hureau C, and Berthoumieu O (2013) Role of metal ions in the self-assembly of the Alzheimer's amyloid-beta peptide. Inorg. Chem 52 (21), 12193–206. [PubMed: 23607830]

(28). Eskici G. z., and Axelsen PH (2012) Copper and Oxidative Stress in the Pathogenesis of Alzheimer's Disease. Biochemistry 51 (32), 6289–6311. [PubMed: 22708607]

(29). Braymer JJ, DeToma AS, Choi J-S, Ko KS, and Lim MH (2011) Recent Development of Bifunctional Small Molecules to Study Metal-Amyloid-β Species in Alzheimer's Disease. Int. J. Alzheimer's Dis 2011, 623051.

(30). Rodríguez-Rodríguez C, Telpoukhovskaia M, and Orvig C (2012) The art of building multifunctional metal-binding agents from basic molecular scaffolds for the potential application in neurodegenerative diseases. Coord. Chem. Rev 256 (19), 2308–2332.

(31). Savelieff MG, Nam G, Kang J, Lee HJ, Lee M, and Lim MH (2019) Development of Multifunctional Molecules as Potential Therapeutic Candidates for Alzheimer's Disease, Parkinson's Disease, and Amyotrophic Lateral Sclerosis in the Last Decade. Chem. Rev 119 (2), 1221–1322. [PubMed: 30095897]

(32). Jones MR, Mathieu E, Dyrager C, Faissner S, Vaillancourt Z, Korshavn KJ, Lim MH, Ramamoorthy A, Wee Yong V, Tsutsui S, Stys PK, and Storr T (2017) Multi-target-directed phenol-triazole ligands as therapeutic agents for Alzheimer's disease. Chem. Sci 8 (8), 5636–5643. [PubMed: 28989601]

(33). Cho H-J, Sharma AK, Zhang Y, Gross ML, and Mirica LM (2020) A Multifunctional Chemical Agent as an Attenuator of Amyloid Burden and Neuroinflammation in Alzheimer's Disease. ACS Chem. Neurosci 11 (10), 1471–1481. [PubMed: 32310630]

(34). Sharma AK, Schultz JW, Prior JT, Rath NP, and Mirica LM (2017) Coordination Chemistry of Bifunctional Chemical Agents Designed for Applications in Cu-64 PET Imaging for Alzheimer's Disease. Inorg. Chem 56 (22), 13801–13814. [PubMed: 29112419]

(35). Beck MW, Derrick JS, Kerr RA, Oh SB, Cho WJ, Lee SJC, Ji Y, Han J, Tehrani ZA, Suh N, Kim S, Larsen SD, Kim KS, Lee JY, Ruotolo BT, and Lim MH (2016) Structure-mechanism-based engineering of chemical regulators targeting distinct pathological factors in Alzheimer's disease. Nat. Commun 7, 13115. [PubMed: 27734843]

(36). Johnston HM, Pota K, Barnett MM, Kinsinger O, Braden P, Schwartz TM, Hoffer E, Sadagopan N, Nguyen N, Yu Y, Gonzalez P, Tircso G, Wu H, Akkaraju G, Chumley MJ, and Green KN (2019) Enhancement of the Antioxidant Activity and Neurotherapeutic Features through Pyridol Addition to Tetraazamacrocyclic Molecules. Inorg. Chem 58 (24), 16771–16784. [PubMed: 31774280]

(37). Sharma AK, Pavlova ST, Kim J, Finkelstein D, Hawco NJ, Rath NP, Kim J, and Mirica LM (2012) Bifunctional Compounds for Controlling Metal-mediated Aggregation of the Aβ_{42} Peptide. J. Am. Chem. Soc 134 (15), 6625–6636. [PubMed: 22452395]

(38). Sharma AK, Kim J, Prior JT, Hawco NJ, Rath NP, Kim J, and Mirica LM (2014) Small Bifunctional Chelators That Do Not Disaggregate Amyloid β Fibrils Exhibit Reduced Cellular Toxicity. Inorg. Chem 53 (21), 11367–11376. [PubMed: 25333939]

(39). DeToma AS, Choi J-S, Braymer JJ, and Lim MH (2011) Myricetin: A Naturally Occurring Regulator of Metal-Induced Amyloid-β Aggregation and Neurotoxicity. ChemBioChem 12 (8), 1198–1201. [PubMed: 21538759]

(40). Porat Y, Abramowitz A, and Gazit E (2006) Inhibition of Amyloid Fibril Formation by Polyphenols: Structural Similarity and Aromatic Interactions as a Common Inhibition Mechanism. Chem. Biol. Drug Des 67 (1), 27–37. [PubMed: 16492146]

(41). Bieschke J, Russ J, Friedrich RP, Ehrnhoefer DE, Wobst H, Neugebauer K, and Wanker EE (2010) EGCG remodels mature α-synuclein and amyloid-β fibrils and reduces cellular toxicity. Proc. Natl. Acad. Sci. U. S. A 107 (17), 7710–7715. [PubMed: 20385841]

(42). Ehrnhoefer DE, Bieschke J, Boeddrich A, Herbst M, Masino L, Lurz R, Engemann S, Pastore A, and Wanker EE (2008) EGCG redirects amyloidogenic polypeptides into unstructured, off-pathway oligomers. Nat. Struct. Mol. Biol 15 (6), 558–566. [PubMed: 18511942]

(43). Lemkul JA, and Bevan DR (2012) Morin Inhibits the Early Stages of Amyloid β-Peptide Aggregation by Altering Tertiary and Quaternary Interactions to Produce "Off-Pathway" Structures. Biochemistry 51 (30), 5990–6009. [PubMed: 22762350]

(44). Sinha S, Du Z, Maiti P, Klärner F-G, Schrader T, Wang C, and Bitan G (2012) Comparison of Three Amyloid Assembly Inhibitors: The Sugar scyllo-Inositol, the Polyphenol Epigallocatechin Gallate, and the Molecular Tweezer CLR01. ACS Chem. Neurosci 3 (6), 451–458. [PubMed: 22860214]

(45). Yang F, Lim GP, Begum AN, Ubeda OJ, Simmons MR, Ambegaokar SS, Chen P, Kayed R, Glabe CG, Frautschy SA, and Cole GM (2005) Curcumin inhibits formation of amyloid β oligomers and fibrils, binds plaques, and reduces amyloid in vivo. J. Biol. Chem 280 (7), 5892–5901. [PubMed: 15590663]

(46). Nam G, Ji Y, Lee HJ, Kang J, Yi Y, Kim M, Lin Y, Lee YH, and Lim MH (2019) Orobol: An Isoflavone Exhibiting Regulatory Multifunctionality against Four Pathological Features of Alzheimer's Disease. ACS Chem. Neurosci 10 (8), 3386–3390. [PubMed: 31199606]

(47). Hyung S-J, DeToma AS, Brender JR, Lee S, Vivekanandan S, Kochi A, Choi J-S, Ramamoorthy A, Ruotolo BT, and Lim MH (2013) Insights into antiamyloidogenic properties of the green tea extract (−)-epigallocatechin-3-gallate toward metal-associated amyloid-β species. Proc. Natl. Acad. Sci. U. S. A 110 (10), 3743–3748. [PubMed: 23426629]

(48). Kang SS, Lee JY, Choi YK, Song SS, Kim JS, Jeon SJ, Han YN, Son KH, and Han BH (2005) Neuroprotective effects of naturally occurring biflavonoids. Bioorg. Med. Chem. Lett 15 (15), 3588–3591. [PubMed: 15978805]

(49). Thapa A, Woo E-R, Chi EY, Sharoar MG, Jin H-G, Shin SY, and Park I-S (2011) Biflavonoids Are Superior to Monoflavonoids in Inhibiting Amyloid-β Toxicity and Fibrillogenesis via Accumulation of Nontoxic Oligomer-like Structures. Biochemistry 50 (13), 2445–2455. [PubMed: 21322641]

(50). Choi EY, Kang SS, Lee SK, and Han BH (2020) Polyphenolic Biflavonoids Inhibit Amyloid-Beta Fibrillation and Disaggregate Preformed Amyloid-Beta Fibrils. Biomol. Ther 28 (2), 145–151.

(51). See the Supporting Information.

(52). Perrin DD (1972)Dissociation constants of organic bases in aqueous solution, Butterworths, London.

(53). Storr T, Merkel M, Song-Zhao GX, Scott LE, Green DE, Bowen ML, Thompson KH, Patrick BO, Schugar HJ, and Orvig C (2007) Synthesis, characterization, and metal coordinating ability of multifunctional carbohydrate-containing compounds for Alzheimer's therapy. J. Am. Chem. Soc 129 (23), 7453–7463. [PubMed: 17511455]

(54). Martell AE, and Smith RM (1976) Critical Stability Constants, p 1, Vol. IV, Plenum, New York.

(55). Hyung SJ, DeToma AS, Brender JR, Lee S, Vivekanandan S, Kochi A, Choi JS, Ramamoorthy A, Ruotolo BT, and Lim MH (2013) Insights into antiamyloidogenic properties of the green tea extract (−)-epigallocatechin-3-gallate toward metal-associated amyloid-beta species. Proc. Natl. Acad. Sci. U. S. A 110 (10), 3743–3748. [PubMed: 23426629]

(56). Bieschke J, Russ J, Friedrich RP, Ehrnhoefer DE, Wobst H, Neugebauer K, and Wanker EE (2010) EGCG remodels mature alpha-synuclein and amyloid-beta fibrils and reduces cellular toxicity. Proc. Natl. Acad. Sci. U. S. A 107 (17), 7710–5. [PubMed: 20385841]

(57). Friesner RA, Banks JL, Murphy RB, Halgren TA, Klicic JJ, Mainz DT, Repasky MP, Knoll EH, Shelley M, Perry JK, Shaw DE, Francis P, and Shenkin PS (2004) Glide: a new approach for rapid, accurate docking and scoring. 1. Method and assessment of docking accuracy. J. Med. Chem 47 (7), 1739–49. [PubMed: 15027865]

(58). Ciudad S, Puig E, Botzanowski T, Meigooni M, Arango AS, Do J, Mayzel M, Bayoumi M, Chaignepain S, Maglia G, Cianferani S, Orekhov V, Tajkhorshid E, Bardiaux B, and Carulla N

(2020) Abeta(1–42) tetramer and octamer structures reveal edge conductivity pores as a mechanism for membrane damage. Nat. Commun 11 (1), 3014. [PubMed: 32541820]

(59). Atrian-Blasco E, Gonzalez P, Santoro A, Alies B, Faller P, and Hureau C (2018) Cu and Zn coordination to amyloid peptides: From fascinating chemistry to debated pathological relevance. Coord. Chem. Rev 371, 38–55.

(60). Biancalana M, and Koide S (2010) Molecular mechanism of Thioflavin-T binding to amyloid fibrils. Biochim. Biophys. Acta, Proteins Proteomics 1804 (7), 1405–1412.

(61). Fagan AM, and Holtzman DM (2010) Cerebrospinal fluid biomarkers of Alzheimer's disease. Biomarkers Med. 4 (1), 51–63.

(62). Lee SJC, Nam E, Lee HJ, Savelieff MG, and Lim MH (2017) Towards an understanding of amyloid-beta oligomers: characterization, toxicity mechanisms, and inhibitors. Chem. Soc. Rev 46 (2), 310–323. [PubMed: 27878186]

(63). Gong YS, Chang L, Viola KL, Lacor PN, Lambert MP, Finch CE, Krafft GA, and Klein WL (2003) Alzheimer's disease-affected brain: Presence of oligomeric A beta ligands (ADDLs) suggests a molecular basis for reversible memory loss. Proc. Natl. Acad. Sci. U. S. A 100 (18), 10417–10422. [PubMed: 12925731]

(64). Walsh DM, and Selkoe DJ (2007) Aβ Oligomers - A Decade of Discovery. J. Neurochem 101 (5), 1172–1184. [PubMed: 17286590]

(65). Haass C, and Selkoe DJ (2007) Soluble Protein Oligomers in Neurodegeneration: Lessons from the Alzheimer's Amyloid b-Peptide. Nat. Rev. Mol. Cell Biol 8 (2), 101–112. [PubMed: 17245412]

(66). Benilova I, Karran E, and De Strooper B (2012) The Toxic Aβ Oligomer and Alzheimer's Disease: An Emperor in Need of Clothes. Nat. Neurosci 15, 349–357. [PubMed: 22286176]

(67). LeVine H (1999) 3rd, Quantification of beta-sheet amyloid fibril structures with thioflavin T. Methods Enzymol. 309, 274–84. [PubMed: 10507030]

(68). Conte-Daban A, Beyler M, Tripier R, and Hureau C (2018) Kinetics Are Crucial When Targeting Copper Ions to Fight Alzheimer's Disease: An Illustration with Azamacrocyclic Ligands. Chem. - Eur. J 24 (33), 8447–8452. [PubMed: 29611877]

(69). Gu M, Bode DC, and Viles JH (2018) Copper Redox Cycling Inhibits Aβ Fibre Formation and Promotes Fibre Fragmentation, while Generating a Dityrosine Aβ Dimer. Sci. Rep 8 (1), 16190. [PubMed: 30385800]

(70). Hindo SS, Mancino AM, Braymer JJ, Liu YH, Vivekanandan S, Ramamoorthy A, and Lim MH (2009) Small Molecule Modulators of Copper-Induced A beta Aggregation. J. Am. Chem. Soc 131 (46), 16663–16664. [PubMed: 19877631]

(71). Gans P, Sabatini A, and Vacca A (1999) Determination of equilibrium constants from spectrophotometric data obtained from solutions of known pH: The program pHab. Ann. Chim 89, 45–49.

(72). Alderighi L (1999) Hyperquad simulation and speciation (HySS): A utility program for the investigaion of equilibria involving soluble and partially soluble species. Coord. Chem. Rev 184, 311.

(73). Klein WL (2002) Aβ toxicity in Alzheimer's disease: globular oligomers (ADDLs) as new vaccine and drug targets. Neurochem. Int 41 (5), 345–352. [PubMed: 12176077]

(74). Lambert MP, Barlow AK, Chromy BA, Edwards C, Freed R, Liosatos M, Morgan TE, Rozovsky I, Trommer B, Viola KL, Wals P, Zhang C, Finch CE, Krafft GA, and Klein WL (1998) Diffusible, nonfibrillar ligands derived from A beta(1–42) are potent central nervous system neurotoxins. Proc. Natl. Acad. Sci. U. S. A 95 (11), 6448–6453. [PubMed: 9600986]

(75). Klein WL (2002) ADDLs & protofibrils - the missing links? Neurobiol. Aging 23 (2), 231–233. [PubMed: 11804707]

(76). Lu JX, Qiang W, Yau WM, Schwieters CD, Meredith SC, and Tycko R (2013) Molecular structure of beta-amyloid fibrils in Alzheimer's disease brain tissue. Cell 154 (6), 1257–68. [PubMed: 24034249]

(77). Gremer L, Scholzel D, Schenk C, Reinartz E, Labahn J, Ravelli RBG, Tusche M, Lopez-Iglesias C, Hoyer W, Heise H, Willbold D, and Schroder GF (2017) Fibril structure of amyloid-beta(1–42) by cryo-electron microscopy. Science 358 (6359), 116–119. [PubMed: 28882996]

(78). Glide, Schrödinger, LLC, New York, 2020 Available from: https://www.schrodinger.com/glide/ (accessed on 2020-01-20).

(79). PyMOL Molecular Graphics System, ver. 2.3., Schrodinger, LLC, New York, 2019.

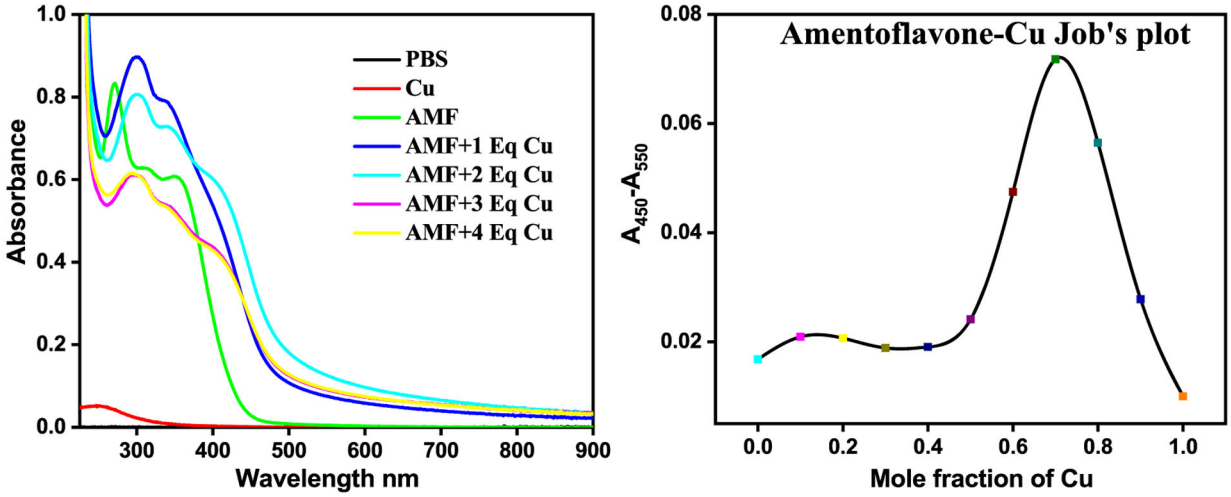

Figure 1.

UV-vis characterization of Cu^{2+} binding to AMF. Left: Spectral changes upon addition of 0–4 equiv of $CuCl_2$ to AMF (25 μM in PBS). Right: Job's plot for AMF and Cu^{2+} in EtOH-PBS (1:10).

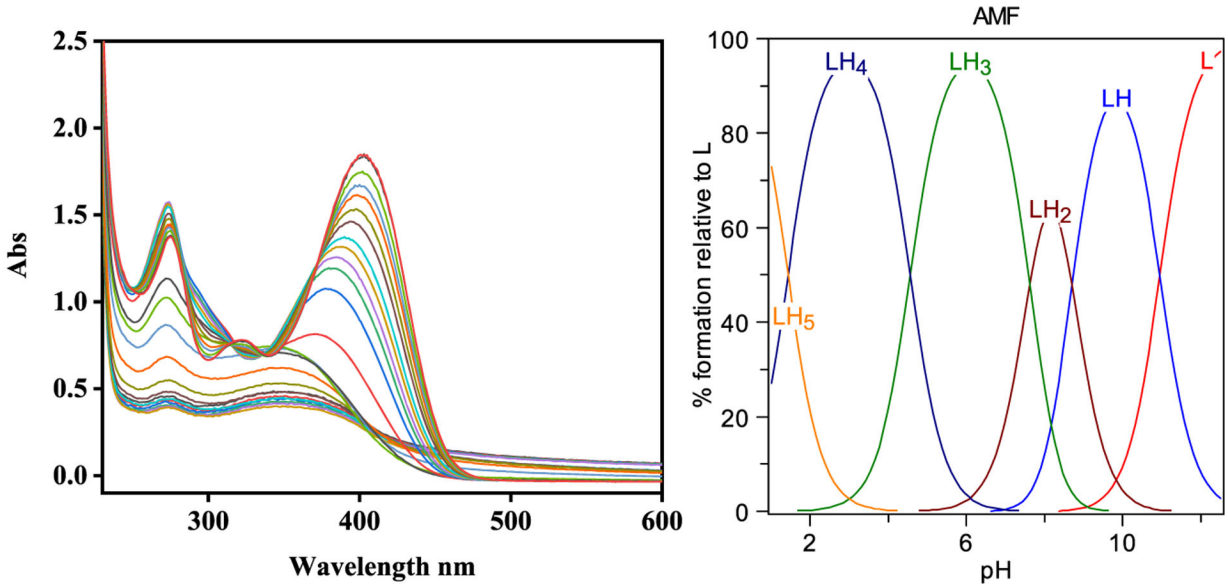

Figure 2.

Variable pH (pH 3–11) UV spectra of AMF ([AMF] = 25 μM; 25 °C, I = 0.1 M NaCl) and species distribution plot, corresponding to the following five pK_a values: 1.42, 4.57, 7.61, 8.71, and 10.96. Neutral AMF corresponds to the LH_4 form.

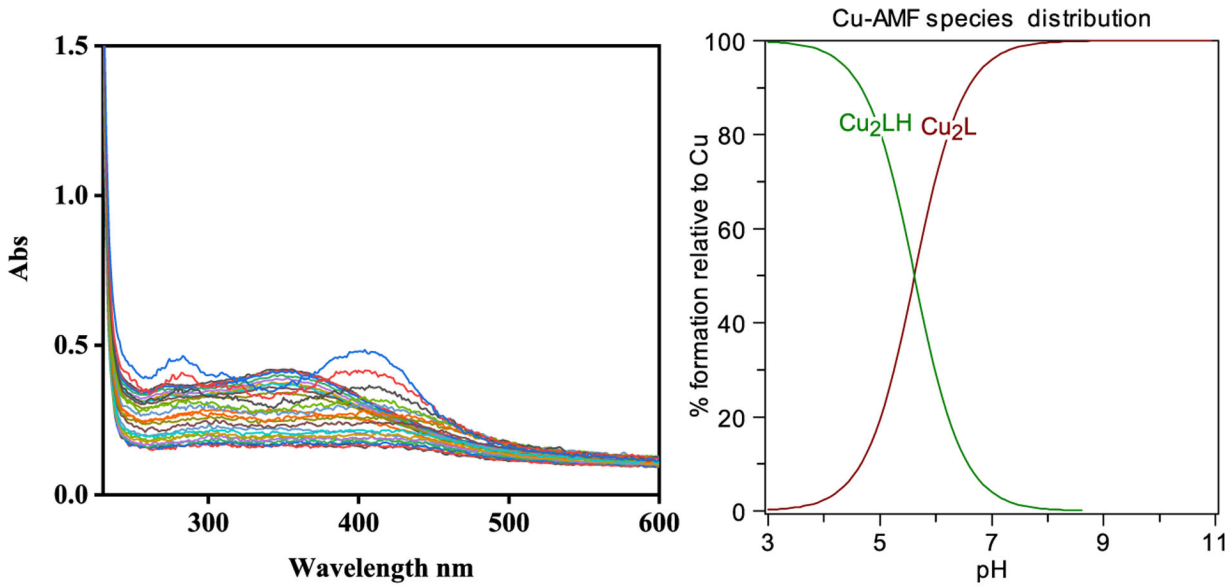

Figure 3.

Variable pH (pH 3–11) UV-vis spectra of AMF and Cu^{2+} spectropotentiometric titration ([AMF] = 25 μM; [Cu^{2+}] = 50 μM, 25 °C, I = 0.1 M NaCl) and species distribution plot (L represents the dideprotonated AMF).

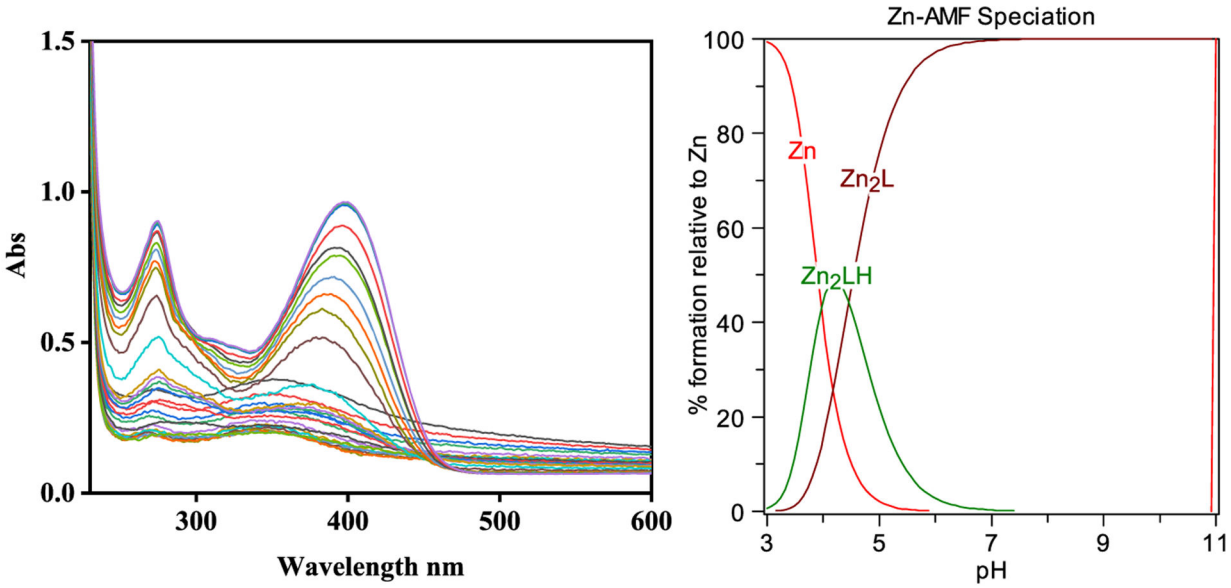

Figure 4.

Variable pH (pH 3–11) UV-vis spectra of AMF and Zn^{2+} spectropotentiometric titration ([AMF] = 25 μM; [Zn^{2+}] = 50 μM, 25 °C, I = 0.1 M NaCl) and species distribution plot (L represents the dideprotonated AMF).

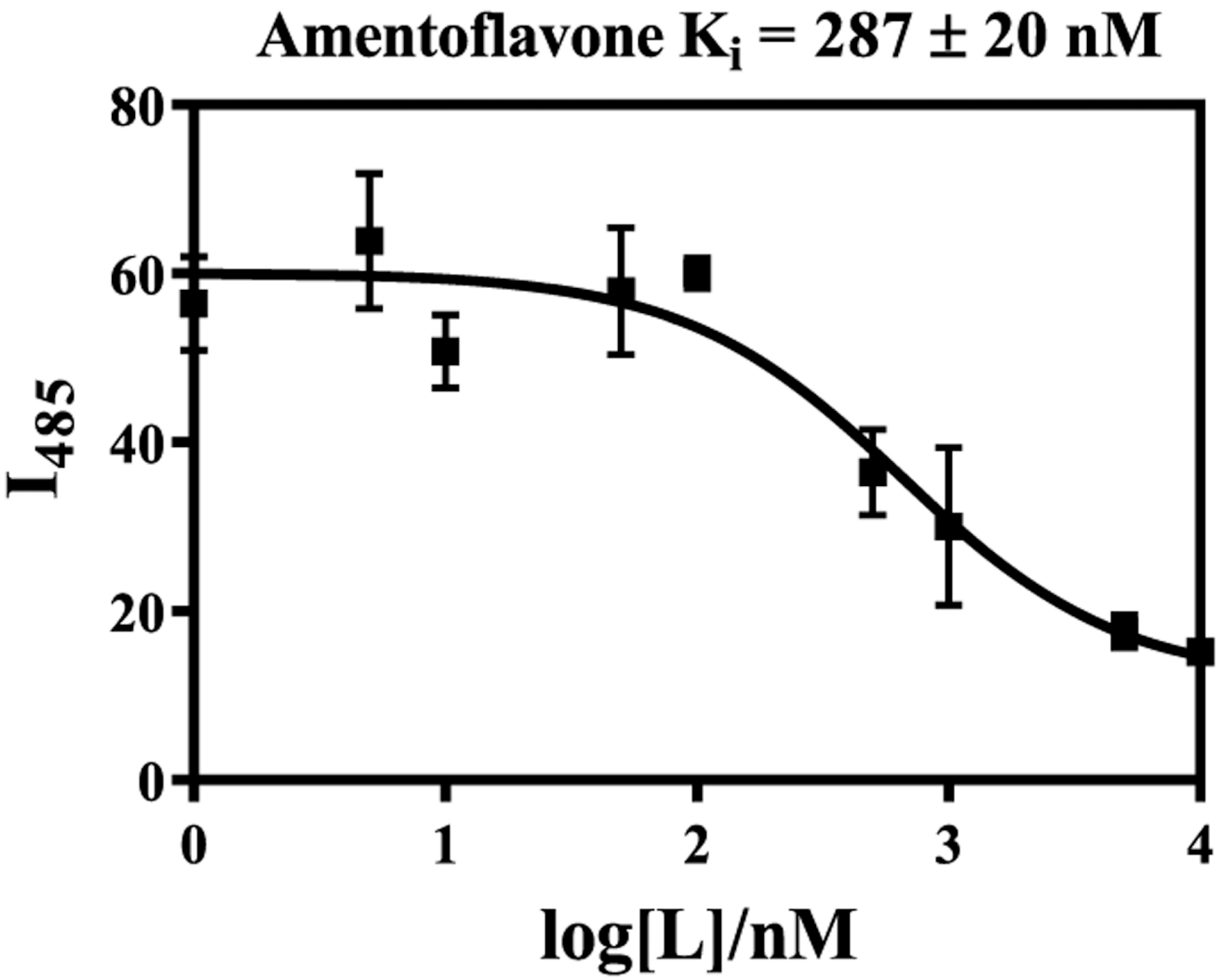

Figure 5.

ThT fluorescence competition assays for AMF ([Aβ] = 2 μM, [ThT] = 1 μM). The error bars represent the standard deviation from three independent experiments.

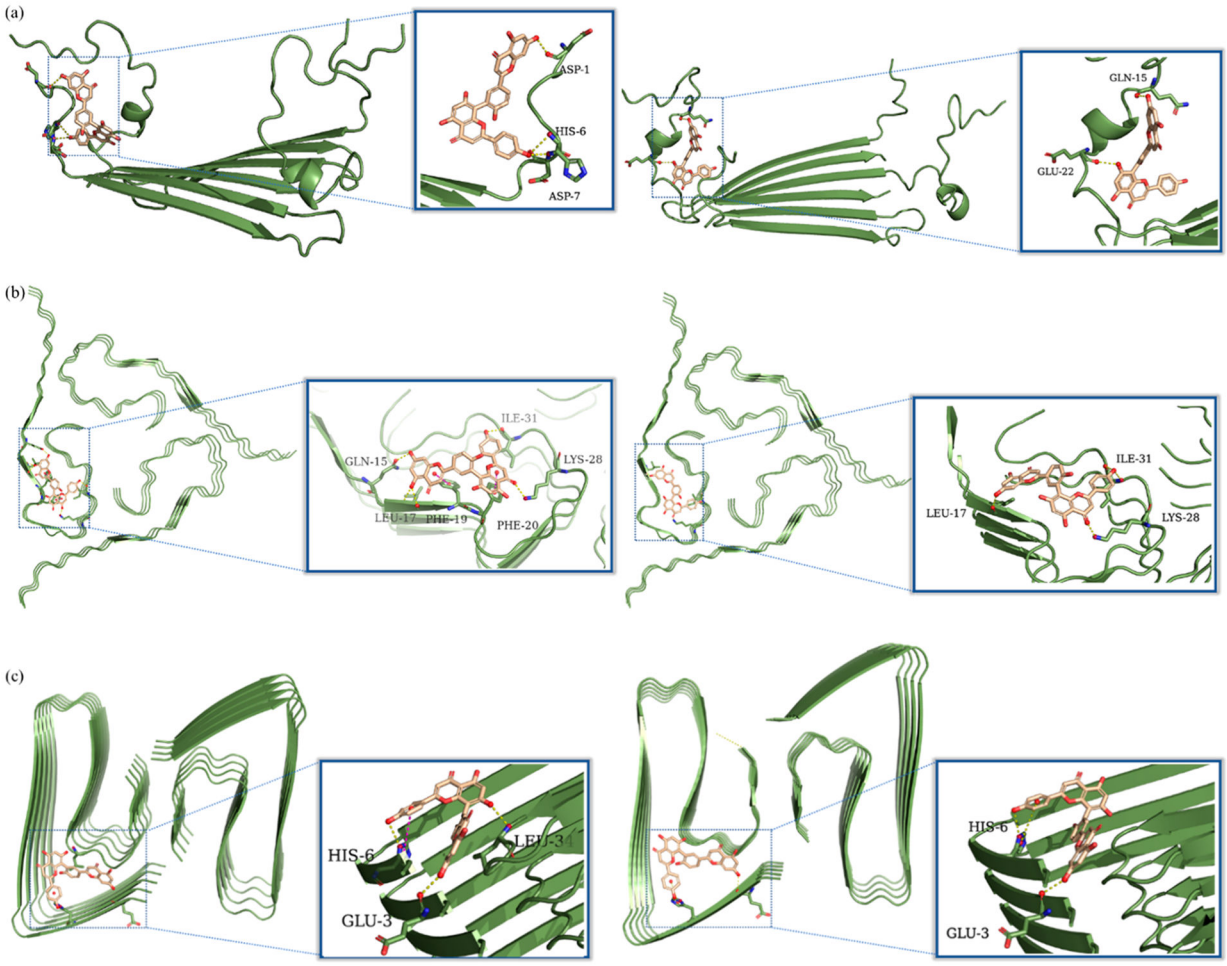

Figure 6.

Calculated binding modes of AMF to various Aβ aggregates: (a) Molecular docking poses of AMF interacting with the Aβ_{42} tetramer (PDB ID: 6RHY). The left figure represents the pose that has the lowest docking score (−4.483), while the right figure represents the pose that has the lowest Glide e-model energy (−65.51 kcal/mol). (b) Molecular docking poses of AMF interacting with the Aβ_{40} fibrils (PDB ID: 2M4J). The left figure represents the pose that has the lowest docking score (−5.198), while the right figure represents the pose that has the lowest Glide e-model energy (−67.03 kcal/mol). (c) Molecular docking poses of AMF interacting with the Aβ_{42} fibrils (PDB ID: 5OQV). The left figure represents the pose that has the lowest docking score (−6.557), while the right figure represents the pose that has the lowest Glide e-model energy (−72.98 kcal/mol). The predicted hydrogen bonds and $\pi-\pi$ interactions are highlighted with yellow and magenta dashed lines.

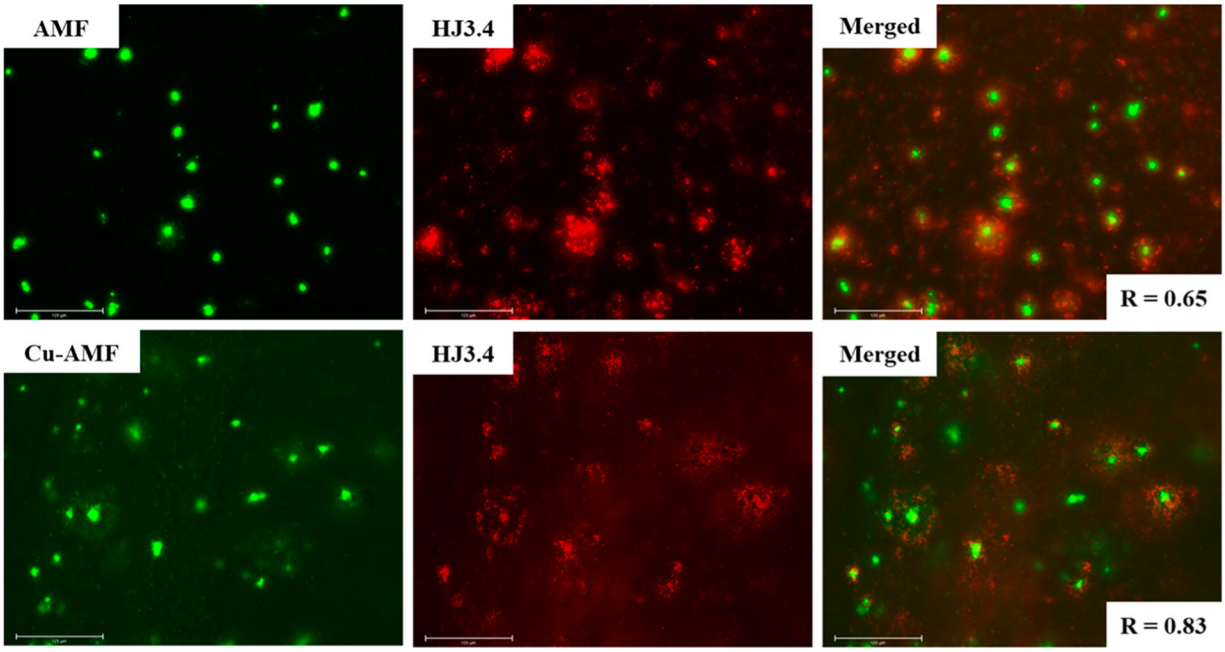

Figure 7.

Fluorescence microscopy images of 5xFAD mice brain sections coincubated with AMF and Cu-AMF (left panels), HJ3.4 antibody (middle panels), and merged images (right panels, along with the Parson's correlation coefficients *R*). Concentrations used: [AMF] = [Cu^{2+}] = 25 μM, [HJ3.4] = 1 μg/mL (scale bar: 125 μm).

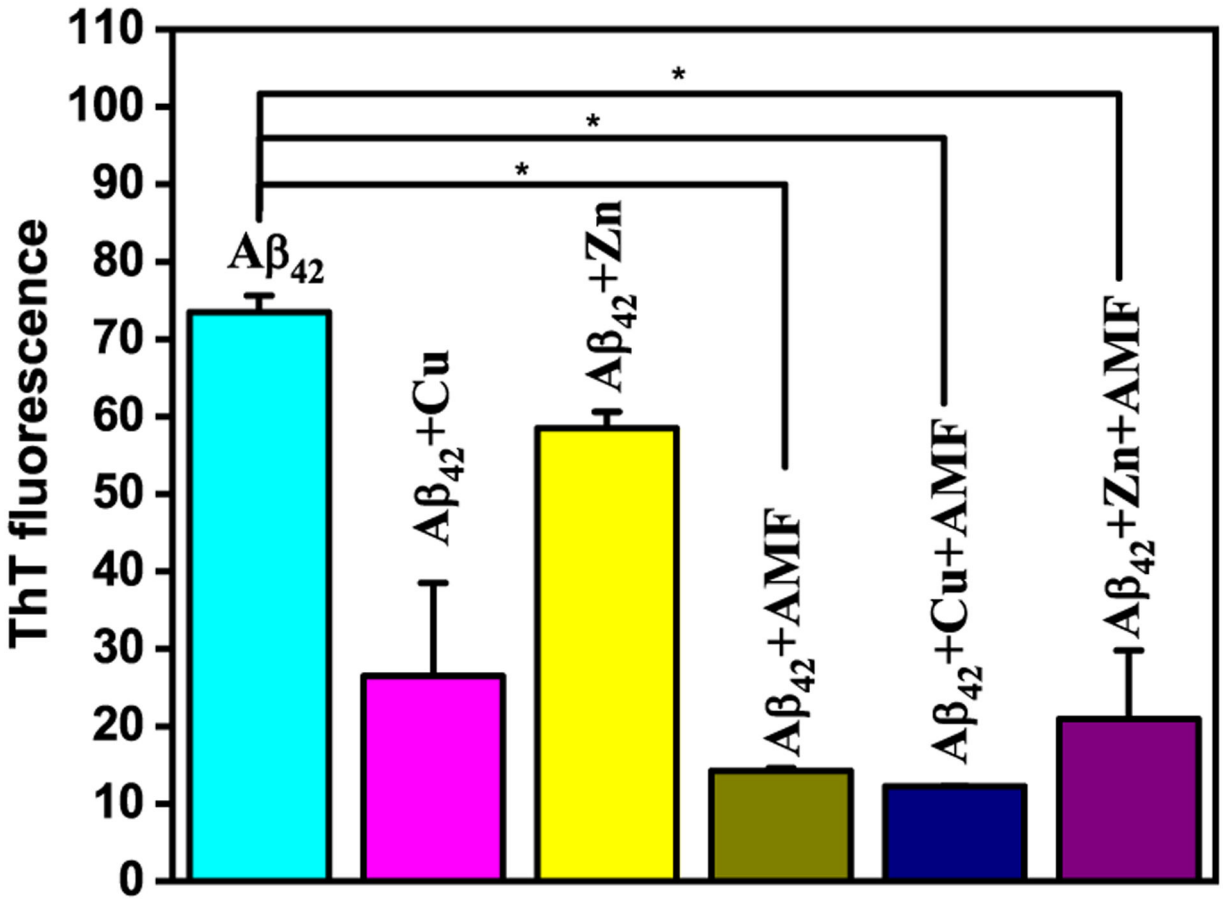

Figure 8.

ThT fluorescence of inhibition of Aβ fibrillization, measured upon incubation at 37 °C for 24 h. Samples are as indicated on top of the lanes (conditions: PBS, [Aβ] = 25 μM; [M^{2+}] = 25 μM; [AMF] = 25 μM). For the ThT fluorescence plate reader measurements, the samples were diluted 10-fold and 10 μM ThT was added to each well. The error bars represent the standard deviation from two independent experiments, and the statistical analysis was evaluated according to one-way ANOVA (*$p < 0.05$).

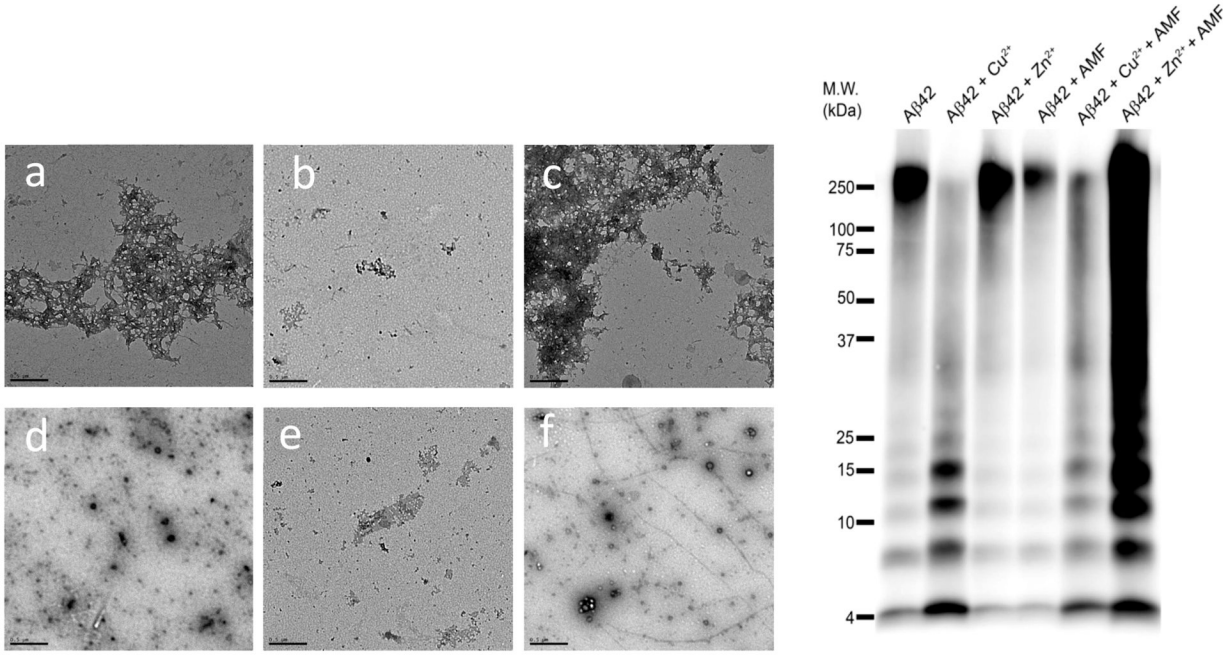

Figure 9.

TEM images and native gel electrophoresis/Western blot for the inhibition of Aβ_{42} aggregation by AMF, in the presence or absence of metal ions ([Aβ_{42}] = [M^{2+}] = 25 μM, [AMF] = 25 μM, 37 °C, 24 h; scale bar = 500 nm). Samples are (a) Aβ_{42}, (b) Aβ_{42} + Cu^{2+}, (c) Aβ_{42} + Zn^{2+}, (d) Aβ_{42} + AMF, (e) Aβ_{42} + Cu^{2+} + AMF, and (f) Aβ_{42} + Zn^{2+} + AMF.

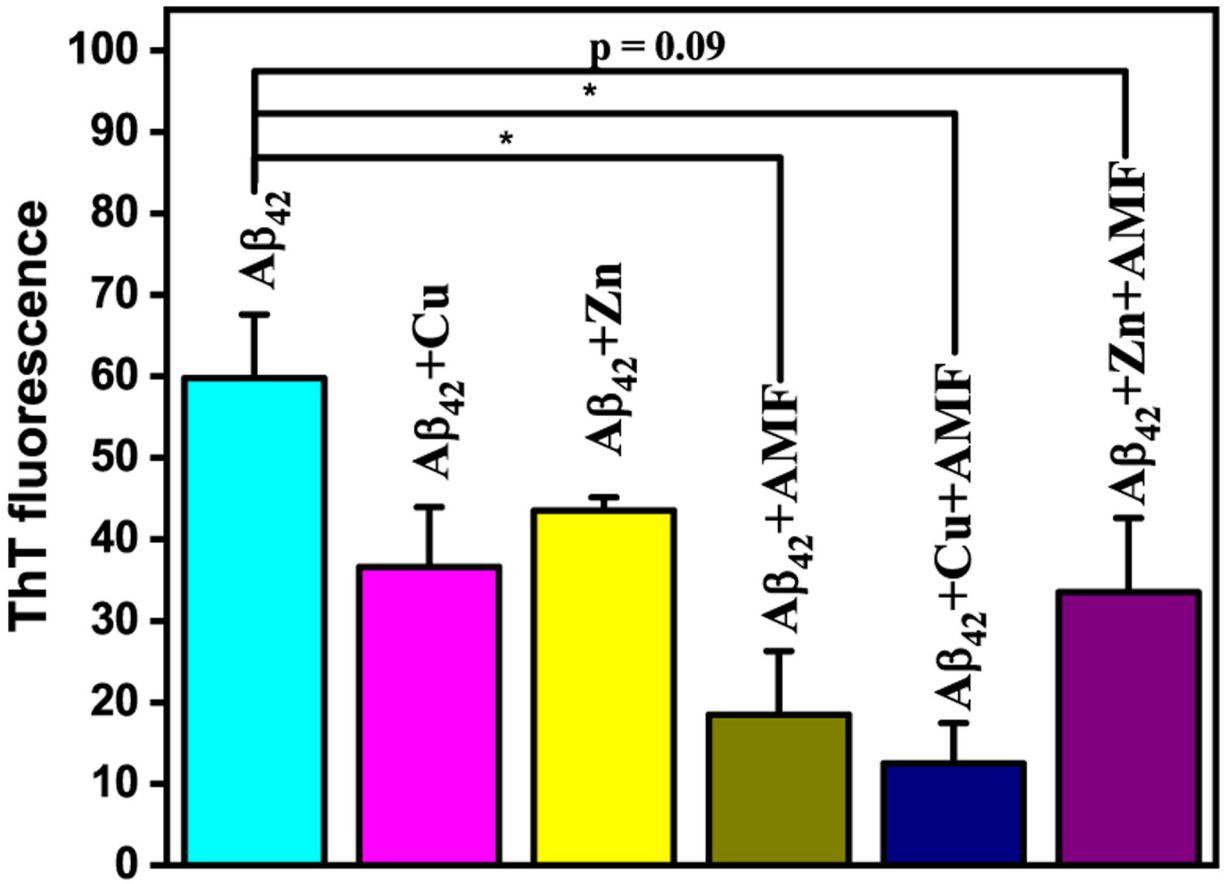

Figure 10.

ThT fluorescence for the disaggregation of Aβ fibrils by AMF, measured upon incubation at 37 °C for 24 h. Samples are as indicated on top of the lanes ([Aβ] = 25 μM; [M^{2+}] = 25 μM; [AMF] = 25 μM). The error bars represent the standard deviation from two independent experiments, and the statistical analysis was evaluated according to one-way ANOVA (*p < 0.05).

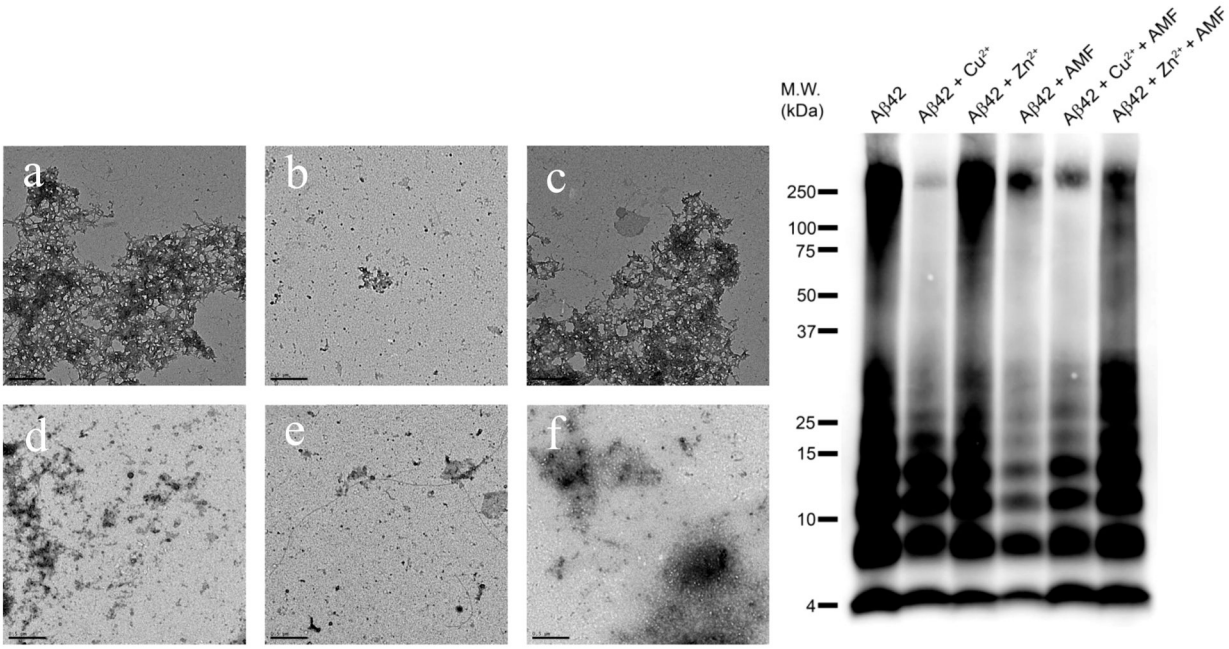

Figure 11.

TEM images and native gel electrophoresis/Western blot for the disaggregation of Aβ_{42} fibrils by AMF in the presence or absence of metal ions (conditions used: [Aβ_{42}] = [M^{2+}] = 25 μM, [AMF] = 25 μM, 37 °C, 24 h for fibrilization with or without metal ions, followed by AMF addition and a further 24 h incubation for disaggregation, scale bar = 500 nm). Samples are (a) Aβ_{42}, (b) Aβ_{42} + Cu^{2+}, (c) Aβ_{42} + Zn^{2+}, (d) Aβ_{42} + AMF, (e) Aβ_{42} + Cu^{2+} + AMF, and (f) Aβ_{42} + Zn^{2+} + AMF.

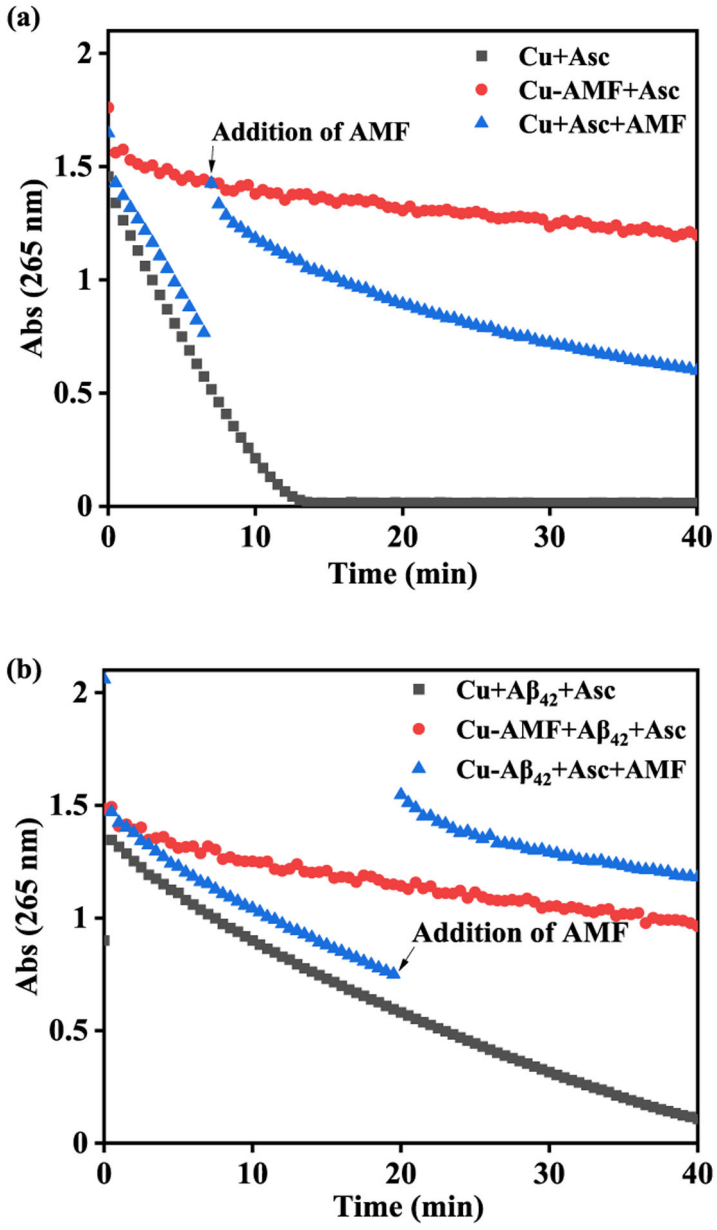

Figure 12.

Kinetics of ascorbate consumption monitored by UV-vis spectroscopy at 265 nm. (a) Cu^{2+} + ascorbate (black), Cu^{2+}-AMF + ascorbate (red), Cu^{2+} + ascorbate + AMF (blue); (b) Cu^{2+}-Aβ_{42} + ascorbate (black), Cu^{2+}-AMF + Aβ_{42} + ascorbate (red), Cu^{2+}-Aβ_{42} + ascorbate + AMF (blue); [Cu^{2+}] = 10 μM, [Aβ_{42}] = 12 μM, [AMF] = 24 μM, [ascorbate] = 100 μM. The large increase in absorbance observed for the blue curves in (a) and (b) likely results from the addition of AMF, which has an absorption band around 265 nm (Figure S1).

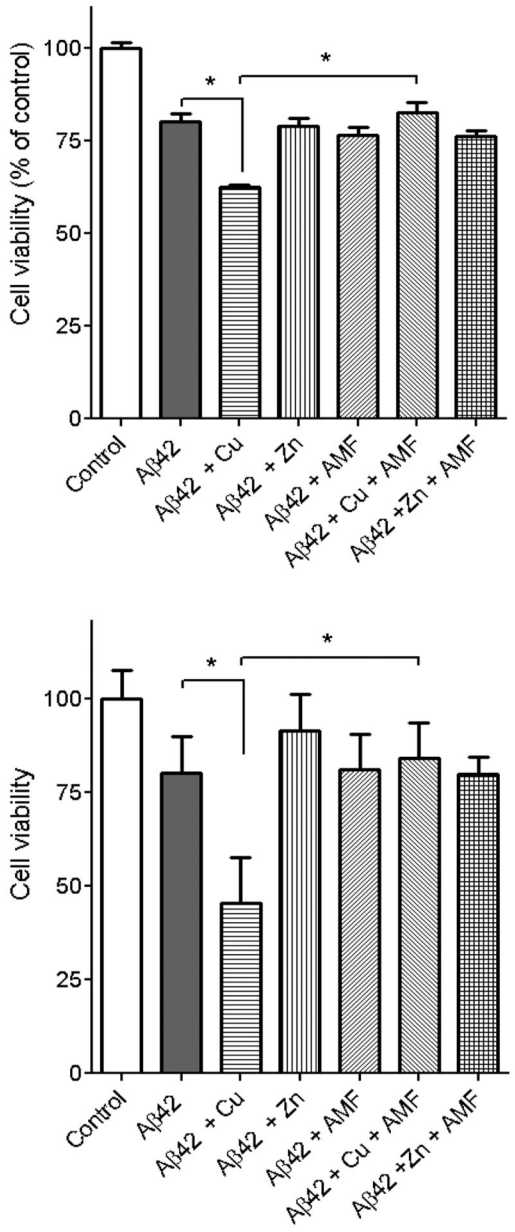

Figure 13.

Cell viability results (% relative to the DMSO control) upon incubation of Neuro2A cells with Aβ_{42} in the presence or absence of metal ions and AMF, under inhibition of Aβ_{42} aggregation (top) and disaggregation of Aβ_{42} fibrils (bottom) conditions. The error bars represent the standard deviation from five independent experiments, and the statistical analysis was evaluated according to one-way ANOVA (*$p < 0.05$).

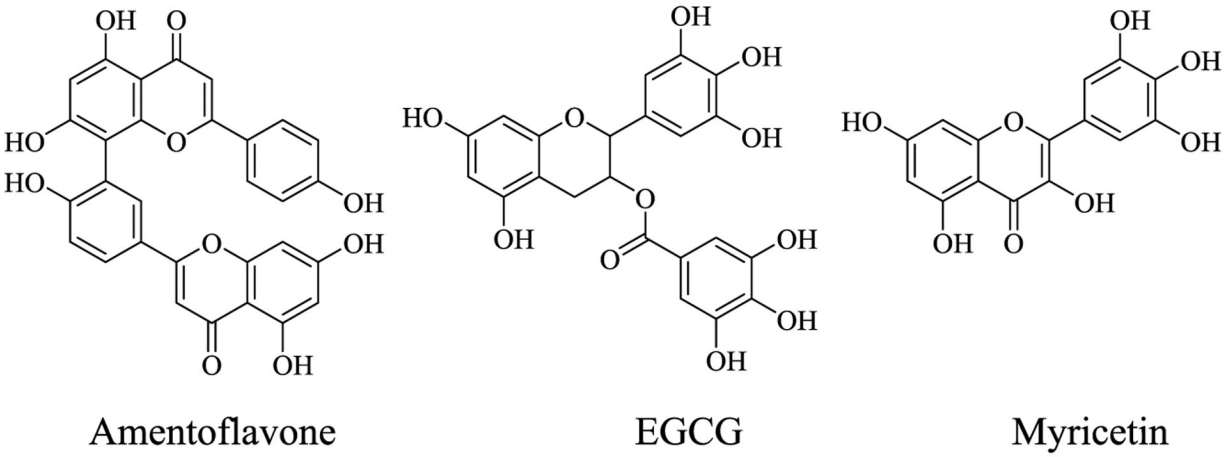

Scheme 1.
Chemical Structures of Amentoflavone (AMF), EGCG, and Myricetin

Table 1.

Stability Constants for AMF:Cu^{2+} and AMF:Zn^{2+} Complexes

metal ion	$2M^{2+} + L = [M_2L]$	$2M^{2+} + LH = [M_2LH]^{+}$
Cu^{2+}	32.5(2)	5.6(2)
Zn^{2+}	25.11(2)	4.46(3)

Table 2.

Calculated pM Values (pM = $-\log[M]_{free}$; M = Zn^{2+}, Cu^{2+}) for a Solution Containing a 2:1 Metal:AMF Mixture ($[M^{2+}]_{tot}$ = 25 μM; $[AMF]_{tot}$ = 50 μM) at a Given pH

pZn	pCu	
pH 7.4	**pH 6.6**	**pH 7.4**
8.15	9.62	10.44